Inorg. Chem. **2005**, *44*, 8368–8378

Primary Photoinduced Processes in Bimetallic Dyads with Extended Aromatic Bridges. Tetraazatetrapyridopentacene Complexes of Ruthenium(II) and Osmium(II)

Claudio Chiorboli,[†] Sandro Fracasso,[‡] Marcella Ravaglia,[‡] Franco Scandola,*[,†,‡] Sebastiano Campagna,*[,§] Kelly L. Wouters,[||] Rama Konduri,[||] and Frederick M. MacDonnell*[,||]

ISOF-CNR, Sezione di Ferrara, 44100 Ferrara, Italy, Dipartimento di Chimica, Università di Ferrara, and INSTM, Sezione di Ferrara 44100 Ferrara, Italy, Dipartimento di Chimica Inorganica, Chimica Analitica e Chimica Fisica, Università di Messina, and INSTM, Sezione di Messina, 98166 Messina, Italy, and Department of Chemistry and Biochemistry, The University of Texas at Arlington, Arlington, Texas 76019

Received June 28, 2005

The photophysics of the binuclear complexes $[(phen)_2M(tatpp)M(phen)_2]^{4+}$, where M = Ru or Os, phen = 1,10-phenanthroline, and tatpp = 9,11,20,22-tetraazatetrapyrido[3,2-*a*:2′3′-*c*:3″,2″-*l*:2‴,3‴]pentacene, has been studied in acetonitrile and dichloromethane by femtosecond and nanosecond time-resolved techniques. The results demonstrate that complexes of different metals have different types of lowest excited state: a tatpp ligand-centered (LC) triplet in the case of Ru(II); a metal-to-ligand charge-transfer (MLCT) triplet state in the case of Os(II). The excited-state kinetics is strongly solvent-dependent. In the Ru(II) system, the formation and decay of the LC state take place, respectively, in 25 ps and ca. 5 ns in CH_3CN and in 0.5 ps and 1.3 μs in CH_2Cl_2. These solvent effects can be rationalized on the basis of a thermally activated decay of the LC state through the upper MLCT state. In the Os(II) system, the formation and decay of the MLCT state take place, respectively, in 3.8 and 60 ps in CH_3CN and in 0.5 and 4 ps in CH_2Cl_2. These effects are consistent with the solvent sensitivity of the MLCT energy, in terms of driving force and energy-gap law arguments. The relevance of these results for the use of ladder-type aromatic bridges as potential molecular wires is discussed.

Introduction

The study of photoinduced processes in covalently linked donor−acceptor systems has been an active area of research for the past 2 decades,[1−6] In dyads, where a donor and an acceptor molecular component are connected by appropriate bridging groups, intercomponent energy or electron-transfer processes can be triggered by light excitation. Sequential photoinduced processes can take place in more complex structures (triads, tetrads, etc.). The study of such processes by time-resolved techniques has been extremely fruitful, in terms of both fundamental knowledge (experimental verification of electron- and energy-transfer theories[1,2,4]) and potential applications (charge separation,[5] antenna effect,[7−9] and other interesting light-induced functions[3]).

Dyads suitable for studies of energy-/electron-transfer generally need rigid bridges to ensure precise structural definition (e.g., donor−acceptor distance, mutual orientation).

* To whom correspondence should be addressed. E-mail: snf@unife.it (F.S.); photochem@chem.unime.it (S.C.); macdonn@uta.edu (F.M.M.).
† ISOF-CNR, Sezione di Ferrara.
‡ Università di Ferrara and INSTM, Sezione di Ferrara.
§ Università di Messina and INSTM, Sezione di Messina.
|| The University of Texas at Arlington.

(1) Wasielewski, M. R.; Niemczyk, M. P.; Svec, W. A.; Pewitt, E. B. *J. Am. Chem. Soc.* **1985**, *107*, 1080−1082.
(2) Paddon-Row, M. N.; Oliver, A. M.; Warman, J. M.; Smit, K. J.; de Haas, M. P.; Oevering, H.; Verhoeven, J. W. *J. Phys. Chem.* **1988**, *92*, 6958−6962.
(3) Balzani, V.; Scandola, F. *Supramolecular Photochemistry*; Horwood: Chichester, U.K., 1991.
(4) Paddon-Row, M. N. In *Electron Transfer in Chemistry*; Balzani, V., Ed.; Wiley-VCH: Weinheim, Germany, 2001; Vol. III, Chapter 2.1, pp 179−271, and references therein.
(5) Gust, D.; Moore, T. A.; Moore A. L. In *Electron Transfer in Chemistry*; Balzani, V., Ed.; Wiley-VCH: Weinheim, Germany, 2001; Vol. III, Chapter 2.2, pp 272−336, and references therein.
(6) Scandola, F.; Chiorboli, C.; Indelli, M. T.; Rampi, M. A. In *Electron Transfer in Chemistry*; Balzani, V., Ed.; Wiley-VCH: Weinheim, Germany, 2001; Vol. III, Chapter 2.3, pp 337−408, and references therein.

10.1021/ic051062z CCC: $30.25
Published on Web 10/05/2005

The role of the bridging groups is not only structural, however, as it has been shown that their nature has profound effects on the electron- and energy-transfer rates.[4,6] Thus the bridges are sometimes indicated, using an appealing similarity, as "molecular wires".[10] In fact, different "conduction" mechanisms may apply in these systems. Two limiting regimes can be considered, depending on the energetics of the system:[4,6] (i) superexchange (energy levels of the bridge far apart from those of the donor/acceptor components, exponential distance dependence); (ii) injection/hopping (bridge levels intermediate between those of donor and acceptor components, weaker distance dependence). Intermediate situations, as well as cases of switching between the two mechanisms, have also been reported.[11] The detailed understanding of the role of the bridge in intramolecular energy-/electron-transfer continues to be a subject of considerable interest.[12,13]

Binuclear complexes are inorganic dyads,[6] where donor and acceptor metal complex units are connected by appropriate bridging ligands. Because of their favorable excited-state and redox properties, metal complex units of the polypyridine type are particularly suited for this type of work. Bridging ligands involving modular spacers, i.e., spacers made of a sequence of individual weakly coupled rigid units, are interesting as, under appropriate synthetic control, they may yield homogeneous families of binuclear complexes suitable for systematic studies of the distance dependence of electron- and/or energy-transfer rates. Notable examples are bridging ligands based on polyphenylene[14,15] and poly(ethynylene-phenylene) spacers.[16] The typical result of such types of studies is an exponential decrease of transfer rates with donor−acceptor distance r_{DA}, $k = k_0 \exp(-\beta r_{DA})$, consistent with a superexchange regime. The specific ability of a given type of bridge as electron/energy "conductor" is represented by the attenuation factor β.

Chart 1

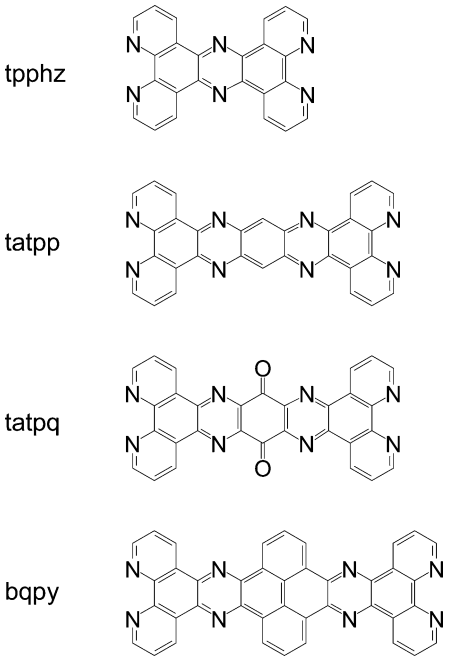

Less studied, though in principle very interesting, are dyads based on fully aromatic fused-ring bridging ligands. Synthetically accessible bridging ligands of this type are the aza-aromatic systems shown in Chart 1.[17−22] Because of the presence of fused pyrazine and phenyl rings as a characteristic motif, these bridges can be loosely termed polyquinoxaline bridges. Although they do contain some structurally repeating units, these bridges cannot be considered to be modular in an electronic sense, as their aromatic π system extends over the entire structure.

From the viewpoint of energy/electron conduction, it is likely that injection into the delocalized system could give high transfer rates and weak distance dependence, i.e, wirelike behavior.

In the past few years, homo- and heteronuclear complexes with the tpphz bridging ligand have been studied in some detail. For homonuclear complexes $[(bpy)_2M(tpphz)M(bpy)_2]^{4+}$ (M = Ru, Os), spectroscopic, electrochemical, and photophysical studies[17,20−22] indicate that two types of MLCT states involving the bridging ligand are present in this complex: $MLCT_1$, with no electron density on the central nitrogens and substantial density on the coordinating atoms, and $MLCT_0$ with substantial electron density on central nitrogens and little density on the coordinating atoms. States

(7) (a) Seth, J.; Palaniappan, V.; Wagner, R. W.; Johnson, T. E.; Lindsey, J. S.; Bocian, D. F. *J. Am. Chem. Soc.* **1996**, *118*, 11194−11207. (b) Hsiao, J.-S.; Krueger, B. P.; Wagner, R. W.; Johnson, T. E.; Delaney, J. K.; Mauzerall, D. C.; Fleming, G. R.; Lindsey, J. S.; Bocian, D. F.; Donohoe, R. J. *J. Am. Chem. Soc.* **1996**, *118*, 11181−11193.
(8) Campagna, S.; Serroni, S.; Puntoriero, F.; Di pietro, C.; Ricevuto, V. In *Electron Transfer in Chemistry*; Balzani, V., Ed.; Wiley-VCH: Weinheim, Germany, 2001; Vol. V, Chapter 1.6, pp 186−214; and references therein.
(9) Ahrens, M. J.; Sinks, L. E.; Rybtchinski, B.; Liu, W.; Jones, B. A.; Giaimo, J. M.; Gusev, A. V.; Goshe, A. J.; Tiede, D. M.; Wasielewski, M. R. *J. Am. Chem. Soc.* **2004**, *126*, 8284−8294.
(10) De Cola, L.; Belser, P In *Electron Transfer in Chemistry*; Balzani, V., Ed.; Wiley-VCH: Weinheim, Germany, 2001; Vol. V, Chapter 1.3, pp 97−136, and references therein
(11) Davis, W. B.; Svec, W. A.; Ratner, M. A.; Wasielewski, M. R. *Nature* **1998**, *396*, 60−63.
(12) Weiss, E. A.; Ahrens, M. J.; Sinks, L. E.; Gusev, A. V.; Ratner, M. A.; Wasielewski, M. R. *J. Am. Chem. Soc.* **2004**, *126*, 5577−5584.
(13) Giacalone, F.; Segura, J. L.; Martin, N.; Guldi, D. M. *J. Am. Chem. Soc.* **2004**, *126*, 5340−5341.
(14) (a) Schlicke, B.; Belser, P.; DeCola, L.; Sabbioni, E.; Balzani, V. *J Am Chem Soc*. **1999**, *121*, 4207−4214. (b) Welter, S.; Benetti, A.; Rot, N.; Salluce, N.; Belser, P.; Sonar, P.; Grimsdale, A. C.; Müllen, K.; Lutz, M.; Spek, A. L.; De Cola, L. *Inorg. Chem*., in press. (c) Welter, S.; Salluce, N.; Belser, P.; Groenefeld, M.; De Cola, L. *Coord. Chem. Rev*., in press.
(15) Chiorboli, C.; Indelli, M. T.; Scandola, F. *Topics Curr. Chem*., in press.
(16) Harriman, A.; Khatyr, A.; Ziessel, R.; Benniston, A. C. *Angew. Chem., Int. Ed*. **2000**, *39*, 4287−4290, and references therein.
(17) Bolger, J.; Gourdon, A.; Ishow, E.; Launay, J.-P. *Inorg. Chem*. **1996**, *35*, 2937−2944.
(18) Ishow, E.; Gourdon, A..; Launay, J.-P.; Lecante, P.; Verlest, M.; Chiorboli, C.; Scandola, F.; Bignozzi, C. A. *Inorg. Chem*. **1998**, *37*, 3603−3609.
(19) Ishow, E.; Gourdon, A.; Launay, J.-P.; Chiorboli, C.; Scandola, F. *Inorg. Chem*. **1999**, *38*, 1504−1510.
(20) Campagna, S.; Serroni, S.; Bodige, S.; MacDonnell, F. M. *Inorg. Chem.* **1999**, *38*, 692−701.
(21) Chiorboli, C.; Bignozzi, C. A.; Scandola, F.; Ishow, E.; Gourdon, A.; Launay, J.-P. *Inorg. Chem.* **1999**, *38*, 2402−2410.
(22) Kim, M.-J.; Konduri, R.; Ye, H.; MacDonnell, F. M.; Puntoriero, F.; Serroni, S.; Campagna, S.; Holder, T.; Kinsel, G.; Rajeshwar, K. *Inorg. Chem*. **2002**, *41*, 2471−2476.

Chart 2

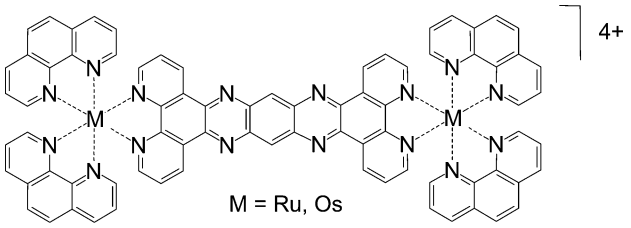

of $MLCT_1$ type are involved in absorption, whereas emission usually takes place from states of $MLCT_0$ type; the emitting states are substantially stabilized in polar solvents, leading to pronounced red shift and lifetime shortening. Recently, direct observation of the $MLCT_1 \rightarrow MLCT_0$ interconversion has been achieved using picosecond[23] and femtosecond[24] time-resolved absorption spectroscopy.[25−27] In heteronuclear complexes, $[(bpy)_2Ru(tpphz)Os(bpy)_2]^{4+/5+}$, the tpphz ligand effectively mediates intercomponent-transfer processes.[24] In the Ru(II)−Os(II) system, energy transfer takes place via a solvent-dependent sequence of steps involving the unoccupied orbitals of the bridge. In the Ru(II)−Os(III) system photoinduced electron transfer proceeds stepwise through the bridging ligand, with some similarities to a charge injection/hopping mechanism.[24]

Recently, some binuclear complexes of tatpp have been synthesized. The homonuclear ruthenium complex, $[(bpy)_2Ru(tatpp)Ru(bpy)_2]^{4+}$, has attracted particular attention as a potential multielectron catalyst. Indeed, $[(phen)_2Ru(tatpp)Ru(phen)_2]^{4+}$ undergoes two reversible electrochemical reductions at moderately negative potentials and is capable of reversibly storing two electrons (and protons) per molecule upon visible light irradiation in the presence of sacrificial reducing agents.[28,29] Aside from these catalytic implications, tatpp complexes deserve attention as potential molecular wires. In particular, a comparison between the photophysics of binuclear tatpp complexes and the shorter tpphz analogues is likely to give important information on the effects of bridge elongation on the electronic properties of the wire. A preliminary account of some photophysical properties of $[(phen)_2Ru(tatpp)Ru(phen)_2]^{4+}$ has been recently published.[30]

In this Article, we present a detailed photophysical study of homonuclear tatpp complexes of Ru(II) and Os(II) (Chart 2). The photophysics of $[(phen)_2Ru(tatpp)Ru(phen)_2]^{4+}$ and $[(phen)_2Os(tatpp)Os(phen)_2]^{4+}$ is investigated by steady-state, nanosecond, and picosecond−femtosecond techniques, in two different solvents (CH_2Cl_2 and CH_3CN). The results are compared with those obtained with the free tatpp ligand (in the form of a zinc adduct). The interpretation of the photophysical results is corroborated by a computational investigation using density functional theory/time-dependent density functional theory (DFT/TDDFT) methods. This study provides a clear picture of the low-lying excited states of these complexes that partially modifies some assignments of a previous preliminary report.[30] The information gained is relevant to the evaluation of these types of polyquinoxaline bridges as possible molecular wires.

Experimental Section

Materials. (a) 9,11,20,22-Tetraazatetrapyrido[3,2-*a*:2′3′-*c*:3″,2″-*l*:2‴,3‴]pentacene (tatpp). The preparation of the tatpp ligand was previously reported.[22] The following additional purification procedure was applied. To a suspension of tatpp (0.3 g, 0.6 mmol) in 150 mL of acetonitrile excess anhydrous zinc(II) tetrafluoroborate (0.86 g, 3.6 mmol) was added, and the mixture was stirred with gentle heating until all of the tatpp dissolved. The warm solution was filtered and to this was added a solution of 1.4 g of Na_2H_2EDTA (EDTA = ethylenediaminetetraacetic acid; 3.8 mmol) in 50 mL of hot H_2O. The resulting solution was gently heated and stirred for 10 min during which time a tan precipitate formed. The precipitate was isolated by filtration and washed with 10−20 mL of hot H_2O. The solid was dried in vacuo at 60 °C overnight.

(b) Zinc Adduct. The ligand was solubilized as described above by addition of 4−5-fold molar excess anhydrous zinc(II) tetrafluoroborate in CD_3CN, for purposes of ^1H NMR characterization. ^1H NMR (2 mM; 500 MHz, MeCN-d_3): δ 9.98 (d, J = 8.3 Hz, 4H), 9.64 (s, 2H), 9.26 (d, J = 5.0 Hz, 4H), 8.33 (dd, J_1 = 8.2 Hz, J_2 = 5.0 Hz, 4H). The highly symmetric ^1H NMR spectrum (four nonequivalent protons, qualitatively identical to that of the tatpp ligand in CD_3CN/trifluoroacetic acid)[22] suggests that the main tatpp/Zn species present in solution, under these conditions, has a 1:2 (tatpp:Zn) stoichiometry. Solutions for absorption and fluorescence spectroscopy, similarly prepared in CH_3CN, are thereafter referred to as solutions of the Zn adduct of tatpp. Isolation of the compound as solid sample was not attempted.

(c) $[(phen)_2Ru(tatpp)Ru(phen)_2][PF_6]_4$. The complex was prepared and purified as previously described.[22,31]

(d) $[(phen)_2Os(tatpp)Os(phen)_2][PF_6]_4$. A mixture of $Os(phen)_2Cl_2$[32] (0.5 g, 8.05 mmol) and tatpp (0.1 g, 2.05 mmol) was suspended in 200 mL of ethanol and 100 mL of water and refluxed for 3 weeks (aerobic environment). After reflux, the mixture was filtered through a bed of Celite and most of the ethanol removed by rotary evaporation. Addition of 20 mL of saturated aqueous NH_4PF_6 resulted in precipitation of the product which was then filtered and washed with 20 mL of hot ethanol (2×) and 30 mL of water (3×).[31] Yield: 0.37 g (83%). ^1H NMR (500 MHz, MeCN-d_3): δ 9.67 (s, 1H), 9.47 (d, J = 8.3 Hz, 2H), 8.44 (dd, J_1 = 0.92 Hz, J_2 = 8.3 Hz, 4H), 8.29 (s, 4H), 8.21 (d, J = 5.0 Hz, 2H), 8.08 (d, J = 5.5 Hz, 2H), 7.93 (d, J = 5.0 Hz, 2H), 7.71 (dd, J_1 = 5.5

(23) Flamigni, L.; Encinas, S.; Barigelletti, F.; MacDonnell, F. M.; Kim, M.-J.; Puntoriero, F.; Campagna, S. *Chem. Commun.* **2000**, 1185−1186.
(24) Chiorboli, C.; Rodgers, M. A. J.; Scandola, F. *J. Am. Chem. Soc.* **2003**, *125*, 483−491.
(25) Alternative views for similar species have also been reported.
(26) Brennaman, M. K.; Alstrum-Acevedo, J. H.; Fleming, C. N.; Jang, P.; Meyer, T. J.; Papanikolas, J. M. *J. Am. Chem. Soc.* **2002**, *124*, 15094−15098.
(27) Pourtois, G.; Beljonne, D.; Moucheron, C.; Schumm, S.; Kirsch-De Mesmaeker, A.; Lazzaroni, R.; Bredas, J.-L. *J. Am. Chem. Soc.* **2004**, *126*, 683−692.
(28) Konduri, R, Ye, H.; MacDonnell, F. M.; Serroni, S.; Campagna, S.; Rajeshwar, K. *Angew. Chem., Int. Ed.* **2002**, *41*, 3185−3187.
(29) Konduri, R.; de Tacconi, N. R.; Rajeshwar, K.; MacDonnell, F. M. *J. Am. Chem. Soc.* **2004**, *126*, 11621−11629.
(30) Chiorboli, C.; Fracasso, S.; Scandola, F.; Campagna, S.; Serroni, S.; Konduri, R.; MacDonnell, F. M. *Chem. Commun.* **2003**, 1658−1659.
(31) As usual for binuclear complexes of this type, the product is a stereoisomeric mixture. The presence of diastereoisomers, however, is expected to be irrelevant in terms of spectroscopic and photophysical behavior. This assumption has been verified in detail, using stereoisomerically pure forms, for the shorter analogue $[(phen)_2Ru(tpphz)Ru(phen)_2]^{4+}$.[20]
(32) Lay, P. A.; Sargenson, A. M.; Taube, H. *Inorg. Synth.* **1986**, *24*, 291.

Hz, J_2 = 8.3 Hz, 2H), 7.65 (dd, J_1 =5.5 Hz, J_2 = 8.3 Hz, 2H), 7.59(dd, J_1 = 5.5 Hz, J_2 = 8.3 Hz, 2H). ^{13}C NMR (CD_3CN-d_3): δ 154.81, 154.10, 152.88, 152.35, 149.92, 149.74, 143.04, 141.20, 136.94, 136.87, 133.18, 131.36, 131.04, 130.56, 128.34, 128.34, 128.13, 126.15. ESI-MS: *m/z* 2023 $[M - PF_6]^+$ 1038 $[M - PF_6]^{2+}$, 939 $[M - 2PF_6]^{2+}$, 866 $[M - 3PF_6]^{2+}$, 622 $[M - 2PF_6]^{3+}$, 469 $[M - 2PF_6]^{4+}$.

Apparatus. Nanosecond transient absorption spectra and lifetimes were measured with an Applied Photophysics laser flash photolysis apparatus, with frequency-doubled (532 nm, 330 mJ), or -tripled (355 nm, 160 mJ), Surelite Continuum II Nd:YAG laser (half-width, 4−6 ns), Photomultiplier (Hamamatsu R928) signals were processed by means of a LeCroy 9360 (600 MHz, 5 Gs/s) digital oscilloscope.

Femtosecond time-resolved experiments were performed using a previously described pump−probe setup,[24] based on the Spectra-Physics Hurricane Ti:sapphire laser source and an Ultrafast Systems Helios spectrometer. The pump pulse was generated by a frequency doubler (400 nm). The probe pulse was obtained by continuum generation on a sapphire plate (useful spectral range, 450−800 nm). The effective time resolution was ca. 300 fs, the temporal chirp over the white-light 450−750 nm range was ca. 200 fs, and the temporal window of the optical delay stage was 0−1000 ps. Time-resolved spectral data were analyzed using Surface Explorer Pro software by Ultrafast Systems.

Cyclic voltammetry (CV) and differential pulse voltammetry (DPV) experiments were performed using a PC-controlled potentiostat (CH Instruments, electrochemical analyzer). A glassy carbon (1.5 mm diameter disk) working electrode from Cypress Systems was used. Immediately before use, the electrodes were polished to a mirror finish with wet alumina (Buehler, 0.05 μm) followed by rinsing with Millipore Milli-Q water, dried, and stored in acetonitrile during the preparation of the electrochemical cell. A Pt wire and a premium "no leak" Ag/ AgCl reference electrode (Cypress, Model EE009) were used as counter and reference electrodes, respectively, and potentials are quoted with respect to this reference. Experiments were conducted in dry acetonitrile (Aldrich, 99.93+%, HPLC grade) with 0.1 M NBu_4PF_6 (Sigma) as supporting electrolyte. Prior to each measurement, the solutions were deoxygenated by bubbling with argon, and this atmosphere was maintained over the electrochemical solution throughout the course of the experiment. The cell ohmic resistance was always compensated. All experiments pertain to the laboratory ambient temperature (20 ± 5 °C).

Computational Methods. Calculations on the electronic ground state of the binuclear model complex $[(bpy)_2Ru(tatpp)Ru(bpy)_2]^{4+}$ were carried out using the B3LYP functional within the density functional theory method.[33] "Double-ζ" quality basis sets were employed for the ligands (6-31G) and the Ru atoms (LANL2DZ). A relativistic effective core potential (ECP) on Ru[34] replaced the inner core electrons, leaving the outer core $[(4s)^2(4p)^6]$ electrons and the $(4d)^6$ valence electrons of Ru(II). The geometry was fully optimized without symmetry constraints. At the ground-state geometry, TDDFT calculations were performed at the same level of accuracy as specified above. Triplet-state unrestricted optimization was carried out using the same approach applied for the ground state.[34,35] Again, no geometry constraints were imposed. All calculations were performed using the Gaussian 98 software package.[36] The program MOLDEN 3.9 was used to visualize the orbitals.[37] A 3D representation of the spin density was plotted with MOLEKEL 4.3.[38]

Results

DFT Calculations. DFT calculations have been performed to obtain relevant molecular orbitals for the ruthenium tatpp complex. For practical reasons, the molecule used in the calculations has bipyridines (bpys) instead of phenanthrolines (phens) as outer ligands. This difference is expected to be of no consequence on the relevant results, however. Many spectroscopic studies, as well as recent theoretical work,[39] confirm the close electronic equivalence of the phen and bpy ligands in ruthenium complexes. Moreover, these ancillary ligands play (see below) a very minor role in the behavior of the binuclear complex as compared with the tatpp bridge. For details of optimized geometries and MO energies, see Supporting Information.

A few of the highest occupied and lowest unoccupied molecular orbitals, calculated at ground-state optimized geometry, are shown in Figure 1. As expected for binuclear complexes of this type, the six closely spaced highest occupied orbitals are essentially metal-centered (combinations of the ruthenium dπ orbitals, one example shown as a contour plot in Figure 1). The next occupied orbital at slightly lower energy is, on the other hand, tatpp-centered. As to the unoccupied orbitals, the LUMO is tatpp-centered with predominant localization in the central ladder-type portion and little electron density on the bpy-like terminal fragments. The next pair of unoccupied orbitals is again tatpp-centered, but with predominant localization on the bpy-like terminal fragments and little electron density on the central ladder-type portion (one of the two orbitals shown as a contour plot in Figure 1, the other one simply differing in the relative signs of the molecular orbital on the two bpy-like fragments).

Absorption Spectra. The absorption spectrum of $[(phen)_2Ru(tatpp)Ru(phen)_2]^{4+}$ in acetonitrile is shown in Figure 2, together with those of $[(phen)_2Os(tatpp)Os(phen)_2]^{4+}$. The absorption spectrum of the tatpp ligand, solubilized by adduct formation (see Experimental Section) with the electronically

(33) (a) Lee, C.; Yang, W.; Parr, R. G. *Phys. Rev. B* **1988**, *37*, 785−789. (b) Becke, A. D. *J. Chem. Phys*. **1993**, *98*, 5648−5652. (c) Hay, P. J. *J. Phys. Chem. A* **2002**, *106*, 1634−1641.
(34) Hay, P. J.; Wadt, W. R. *J. Chem. Phys*. **1985**, *82*, 299−310.
(35) Guillemoles, J. F.; Barone, V.; Joubert, L.; Adamo, C. *J. Phys. Chem. A* **2002**, *106*, 11354−11360.
(36) Frisch, M. J.; Trucks, G. W.; Schlegel, H. B.; Scuseria, G. E.; Robb, M. A.; Cheeseman, J. R.; Zakrzewski, V. G.; Montgomery, J. A.; Stratmann, R. E.; Burant, J. C.; Dapprich, S.; Millam, J. M.; Daniels, A. D.; Kudin, K. N.; Strain, M. C.; Farkas, O.; Tomasi, J.; Barone, V.; Cossi, M.; Cammi, R.; Mennucci, B.; Pomelli, C.; Adamo, C.; Clifford, S.; Ochterski, J.; Petersson, G. A.; Ayala, P. Y.; Cui, Q.; Morokuma, K.; Malick, D. K.; Rabuck, A. D.; Raghavachari, K.; Foresman, J. B.; Cioslowski, J.; Ortiz, J. V.; Stefanov, B. B.; Liu, G.; Liashenko, A.; Piskorz, P.; Komaromi, I.; Gomperts, R.; Martin, R. L.; Fox, D. J.; Keith, T.; Al-Laham, M. A.; Peng, C. Y.; Nanayakkara, A.; Gonzalez, C.; Challacombe, M.; Gill, P. M. W.; Johnson, B. G.; Chen, W.; Wong, M. W.; Andres, J. L.; Head-Gordon, M.; Replogle, E. S.; Pople, J. A. *Gaussian 98*, revision A.11; Gaussian, Inc.: Pittsburgh, PA, 1998.
(37) Schaftenaar, G.; Noordik, J. H. Molden: A Pre- and Post-processing Program for Molecular and Electronic Structures. *J. Comput.-Aided Mol. Des.* **2000**, *14*, 123−134.
(38) (a) Flükiger, H. P.; Lüthi, S.; Portmann, J.; Weber, P. *MOLEKEL 4.3*; Swiss Center for Scientific Computing: Manno, Switzerland, 2000−2002. (b) Portmann, S.; Lüthi, H. P. MOLEKEL: An Interactive Molecular Graphics Tool. *Chimia* **2000**, *54*, 766−770.
(39) (a) Zheng, K. C.; Wang, J. P.; Liu, X. W.; Shen, Y.; Yun, F. C. *THEOCHEM* **2002**, *577*, 95−105. (b) Zheng, K. C.; Wang, J. P.; Peng, W. L.; Liu, X. W.; Yun, F. C. *THEOCHEM* **2002**, *582*, 1−9.

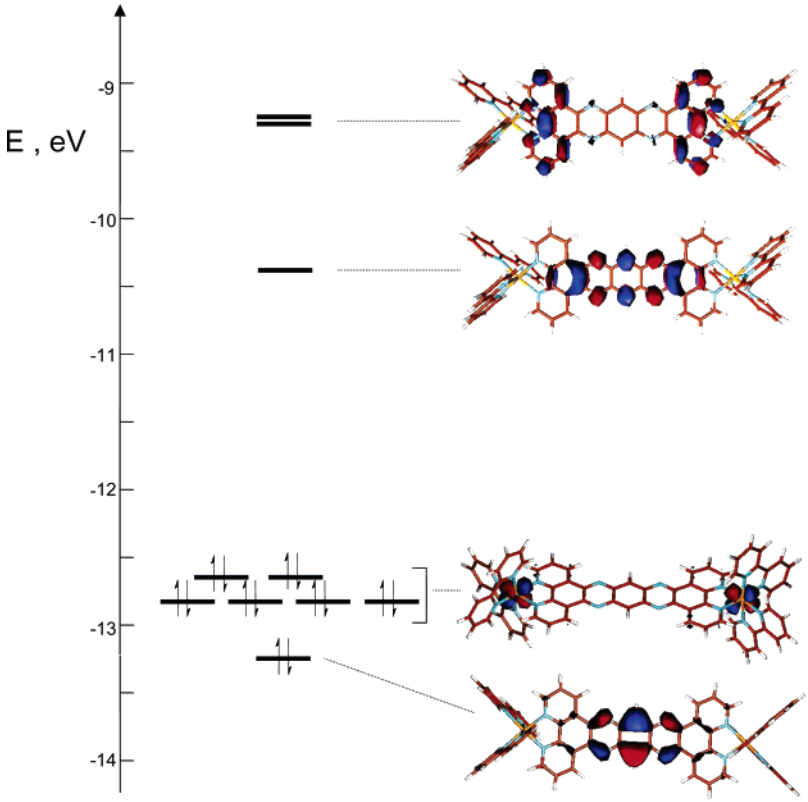

Figure 1. Energies and sample contour plots of some of the highest occupied and lowest unoccupied molecular orbitals of $[(bpy)_2Ru(tatpp)Ru(bpy)_2]^{4+}$ from DFT calculations.

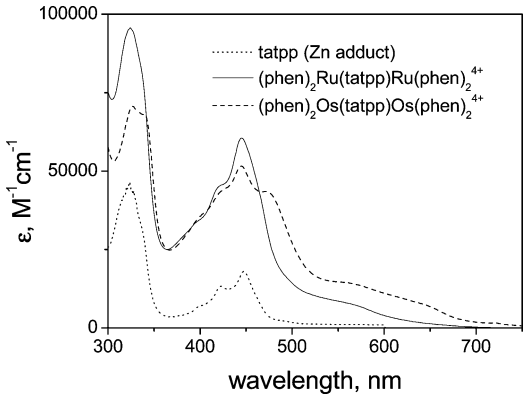

Figure 2. Absorption spectra of $[(phen)_2Ru(tatpp)Ru(phen)_2]^{4+}$, $[(phen)_2Os(tatpp)Os(phen)_2]^{4+}$, and tatpp ($Zn^{2+}$ adduct) in CH_3CN.

innocent Zn metal, is also shown for comparison. In the visible absorption spectra, the sharp structured feature with a maximum at 450 nm is clearly due to tatpp-centered absorption. The underlying broad band system spectrum is characteristic of MLCT absorption. As usual, the MLCT bands of the osmium complex are slightly red-shifted with respect to the ruthenium analogue. Also, relatively intense spin-forbidden MLCT bands are present for the osmium complex in the low-energy region.

The absorption spectra of the complexes do not change appreciably by changing the solvent from CH_3CN to CH_2Cl_2.

Electrochemistry. The electrochemical properties in CH_3CN of $[(phen)_2Ru(tatpp)Ru(phen)_2]^{4+}$ and $[(phen)_2Os(tatpp)Os(phen)_2]^{4+}$ are summarized in Table 1. For a detailed description of the electrochemical experiments, the reader is referred to ref 29. Data for $[(phen)_2Ru(tpphz)Ru(phen)_2]^{4+}$, $[(phen)_2Os(tpphz)Os(phen)_2]^{4+}$, $Ru(bpy)_3^{2+}$, and $Os(bpy)_3^{2+}$ are included for purposes of comparison.

Oxidation takes place, as usual for metal polypyridine complexes, at the metal center. Consistent with a weak metal−metal interaction, it appears as a single two-electron process. As usual, the Os system is easier to oxidize than the Ru one: the difference (0.47 V) is comparable to that of tpphz complexes (0.45 V). In reduction, the first and second one-electron processes of the Ru(II) tatpp complex, as well as the two-electron process, have been assigned to reduction of the tatpp bridging ligand.[29] An analogous assignment is here proposed for the Os(II) species. By comparison with the tpphz analogues, the distinctive features of the tatpp complexes are as follows: (i) much easier first reduction (by 0.45 V for Ru and 0.63 V for Os); (ii) two one-electron reduction processes, instead of one. Both one-electron reduction processes for the Os tatpp dimer are considerably more positive than for the Ru tatpp dimer with a positive shift of 0.19 V for the first reduction and 0.51 V for the second one.

Photophysics. Photophysical experiments on $[(phen)_2Ru(tatpp)Ru(phen)_2]^{4+}$ and $[(phen)_2Os(tatpp)Os(phen)_2]^{4+}$ were performed in two solvents, CH_3CN and CH_2Cl_2. For purposes of comparison, the photophysics of the tatpp bridging ligand, solubilized by complexation with Zn^{2+} in CH_3CN (see Experimental Section), was also studied.

$[(phen)_2Ru(tatpp)Ru(phen)_2]^{4+}$. The complex does not show any appreciable emission in solution at $\lambda \leq 900$ nm.

Table 1. Electrochemical Properties of the Ruthenium and Osmium Tatpp Complexes. Data for Related Species Included for Comparison

complex	E_{ox}[a]	$E_{red(1)}$[a]	$E_{red(2)}$[a]	$E_{red(3)}$[a]
$[(phen)_2Ru(tatpp)Ru(phen)_2]^{4+}$	+1.32 [2][b]	−0.26 [1][b]	−0.75 [1][b]	−1.32 [2][b]
$[(bpy)_2Ru(tpphz)Ru(bpy)_2]^{4+}$	+1.34 [2][c]	−0.71 [1][c]	−1.31 [2][c]	
$Ru(bpy)_3^{2+}$	+1.27 [1][c]	−1.31[1][c]	−1.50[1][c]	
$[(phen)_2Os(tatpp)Os(phen)_2]^{4+}$	+0.85 [2][d]	−0.07[1][d]	−0.24 [1][d]	−1.27 [2][d]
$[(bpy)_2Os(tpphz)Os(bpy)_2]^{4+}$	+0.89 [2][c]	−0.70 [1][c]	−1.21 [2][c]	
$Os(bpy)_3^{2+}$	+0.78 [1][c]	−1.30[1][c]	−1.48[1][c]	

[a] V vs SCE, number of transferred electrons in brackets. [b] From ref 29, converted to SCE from Ag/AgCl (by adding −0.04 V). [c] From ref 17. [d] This work.

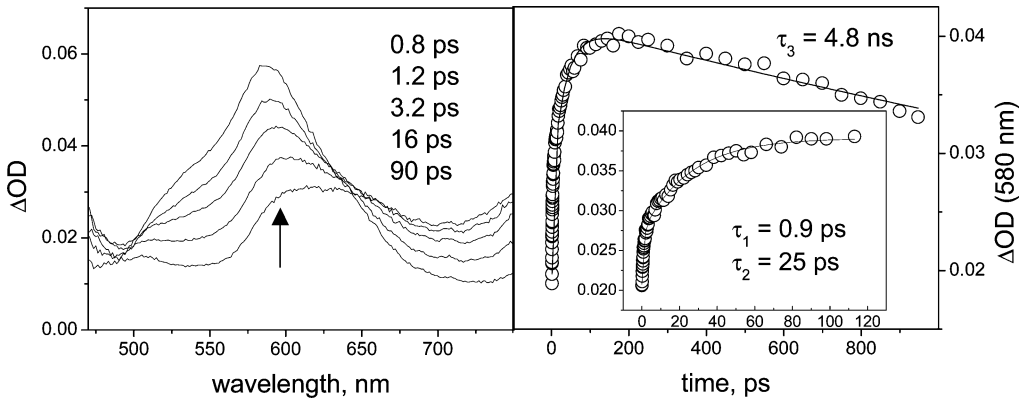

Figure 3. Transient spectral changes (left) and kinetics (right) observed in ultrafast spectroscopy for $[(phen)_2Ru(tatpp)Ru(phen)_2]^{4+}$ in CH_3CN.

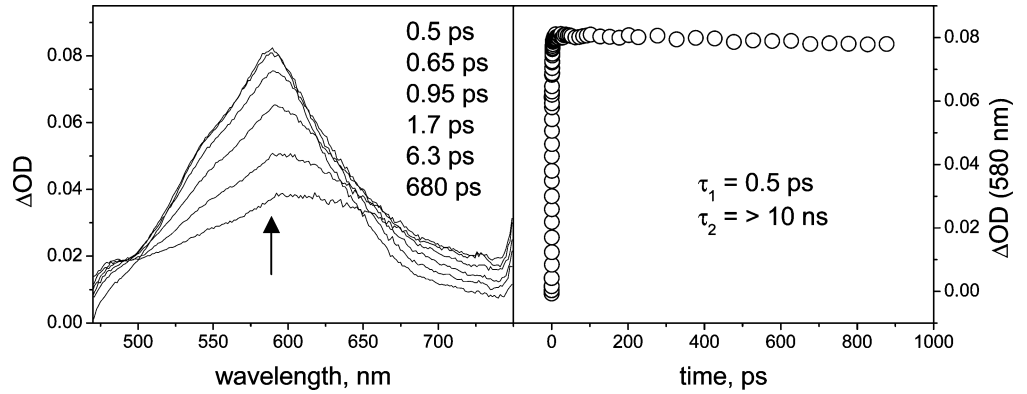

Figure 4. Transient spectral changes (left) and kinetics (right) observed in ultrafast spectroscopy for $[(phen)_2Ru(tatpp)Ru(phen)_2]^{4+}$ in CH_2Cl_2.

It shows, on the other hand, transient spectral changes in the picosecond−nanosecond time domain.

The transient behavior observed in CH_3CN by ultrafast spectroscopy is shown in Figure 3. A prominent band with maximum at 580 nm is observed to develop within 100 ps after light excitation, with complex kinetics involving a major (ca. 65%) component of 25 ps. The transient starts to decay slowly within the temporal window of the experiment, with an apparent lifetime of ca. 5 ns. Consistent with this estimate, no transient can be observed after 10 ns in laser flash photolysis experiments.

The transient behavior observed in CH_2Cl_2 is shown in Figure 4. The spectral changes are similar to those observed in CH_3CN, characterized again by formation of the 580 nm band. The kinetics is different, however. The formation is faster than in CH_3CN (almost limited by instrumental rise time; apparent time constant, 0.5 ps). On the other hand, no decay is observed over the time window of the experiment, indicating a lifetime greater than 10 ns. Consistent with this estimate, the same transient can be observed in laser flash photolysis (Figure 5), with a lifetime of 1.3 μs in deaerated solution (0.5 μs in air-equilibrated solution).

$[(phen)_2Os(tatpp)Os(phen)_2]^{4+}$. The complex does not show any appreciable emission in solution at $\lambda \leq 900$ nm. It shows, on the other hand, transient spectral changes in the picosecond time domain.

The transient behavior observed in CH_3CN by ultrafast spectroscopy is shown in Figure 6. The spectral changes are complex and quite different from those observed for the ruthenium system. A first process is observed (Figure 6, upper part) as a very fast decrease in optical density in the 500−560 nm range (time constant, 0.45 ps). The resulting transient spectrum decays in a subsequent process to the initial baseline (Figure 6, lower part), with time constant ca. 5 ps. As expected, no transient is observed in laser flash photolysis experiments (time delay $\geq$ 10 ns).

The behavior in CH_2Cl_2 is qualitatively very similar (Figure 7). The main difference with respect to CH_3CN lies

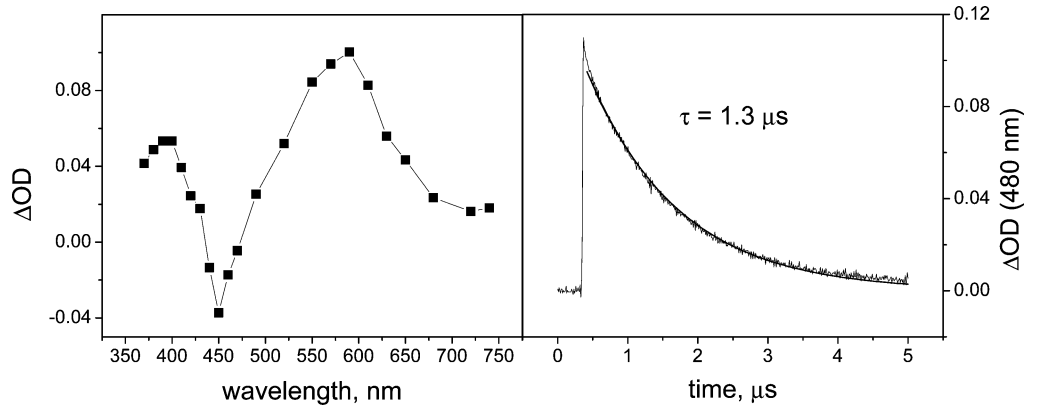

Figure 5. Laser flash photolysis of $[(phen)_2Ru(tatpp)Ru(phen)_2]^{4+}$ in CH_2Cl_2. Transient spectrum recorded at 50 ns delay (left); decay kinetics (right).

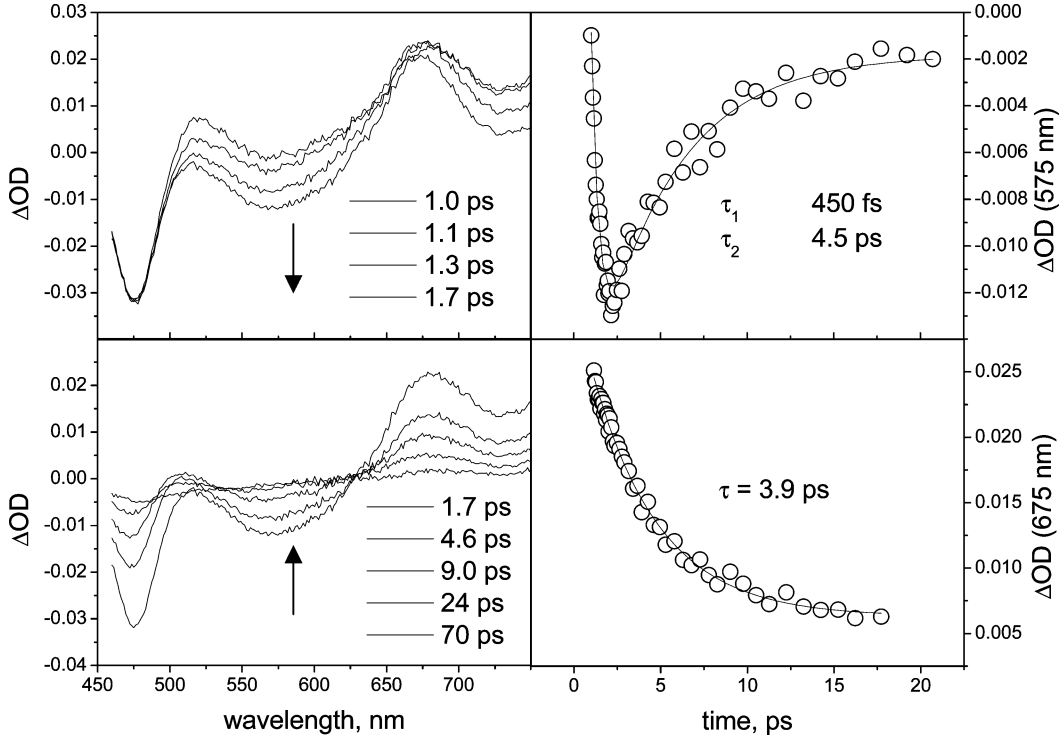

Figure 6. Transient spectral changes (left) and kinetics (right) observed in ultrafast spectroscopy for $[(phen)_2Os(tatpp)Os(phen)_2]^{4+}$ in CH_3CN.

in the kinetics, which is slower for both the first (time constant, ca. 3.8 ps) and the second process (time constant, ca. 60 ps).

Zn Adduct. In CH_3CN, the Zn adduct of the tatpp ligand exhibits a weak, structured fluorescence (λ_{max}, 547 nm) with an excitation spectrum that closely matches the absorption spectrum of Figure 2. Its low intensity (Φ = ca. 0.01) and long lifetime (τ = 4 ns), however, suggest that this emission is due to minor[40,41] amounts of free (Zn uncomplexed) ligand.

The spectral changes observed in ultrafast spectroscopy are shown in Figure 8. A transient spectrum with sharp maximum at 590 nm and a shoulder at ca. 700 nm, instantaneously formed within the excitation pulse, decays with 139 ps lifetime. The constant spectrum reached at the end of this decay process is similar but not identical to the initial one (maximum at 575 nm, lack of long wavelength shoulder). This transient absorption persists for much longer times, as shown by the flash photolysis results reported in Figure 9. The lifetime in deaerated solution is 30 μs (260 ns in air-equilibrated solution).

Discussion

Spectroscopic and Electrochemical Properties. The visible spectra of the complexes (Figure 2) clearly consist of the superposition of the structured absorption of the tatpp ligand and the broad MLCT absorption characteristic of ruthenium(II) and osmium(II) polypyridine chromophores. An interesting question arises, however, when these spectra are considered in the light of the redox properties of the complexes (Table 1). To make the point, we focus on the Ru(II) system. It is well-known that in Ru(II) complexes the energies of MLCT absorption correlate linearly with the

(40) Estimated in few percent, by comparison of the apparent radiative rate constant (of the order of 10^6 s^{-1}) with the value expected[41] from the intensity of the corresponding absorption band (of the order of 10^8 s^{-1}).

(41) Strickler, S. J.; Berg, R. A. *J. Chem. Phys.* **1962**, *37*, 814−822.

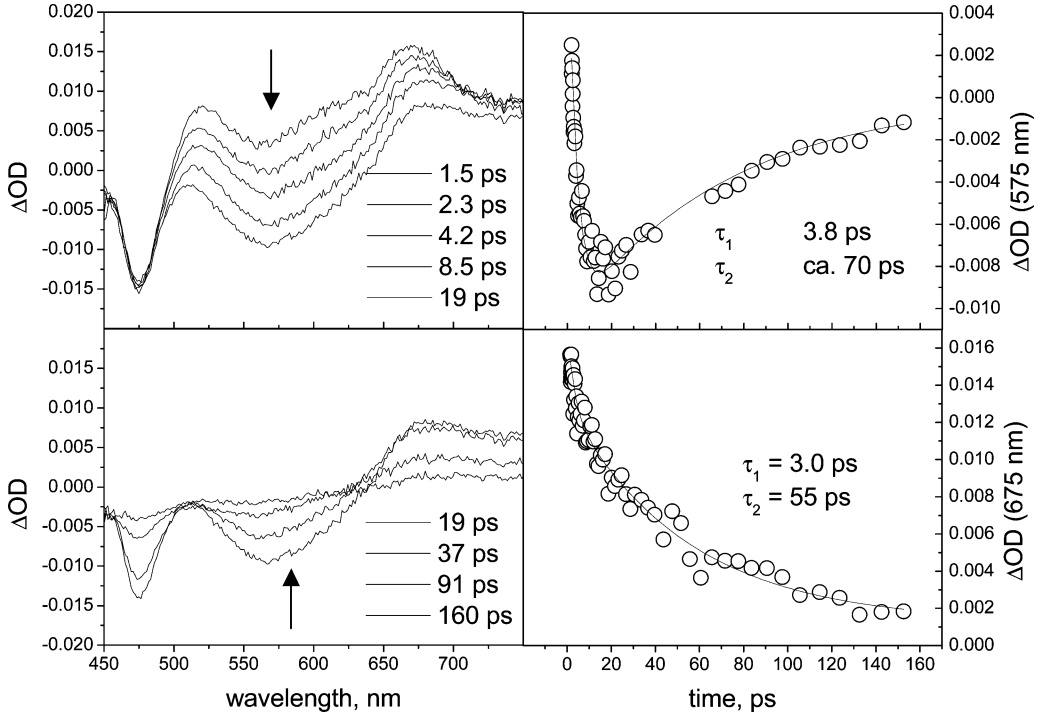

Figure 7. Transient spectral changes (left) and kinetics (right) observed in ultrafast spectroscopy for $[(phen)_2Os(tatpp)Os(phen)_2]^{4+}$ in CH_2Cl_2.

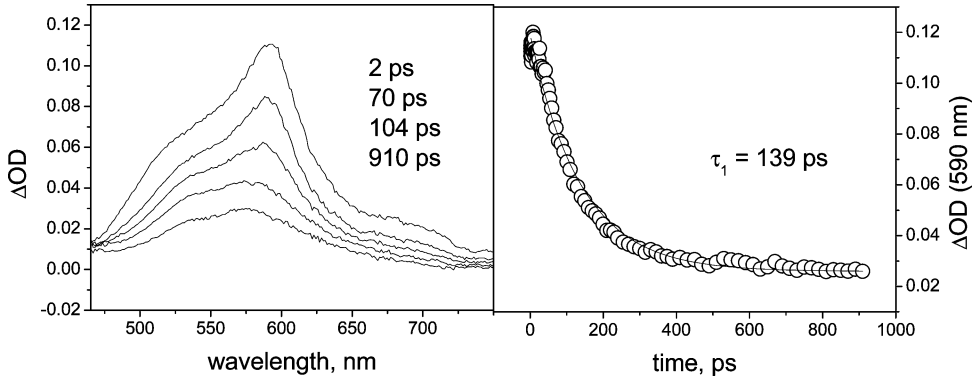

Figure 8. Transient spectral changes (left) and kinetics (right) observed in ultrafast spectroscopy of the Zn−tatpp complex in CH_3CN.

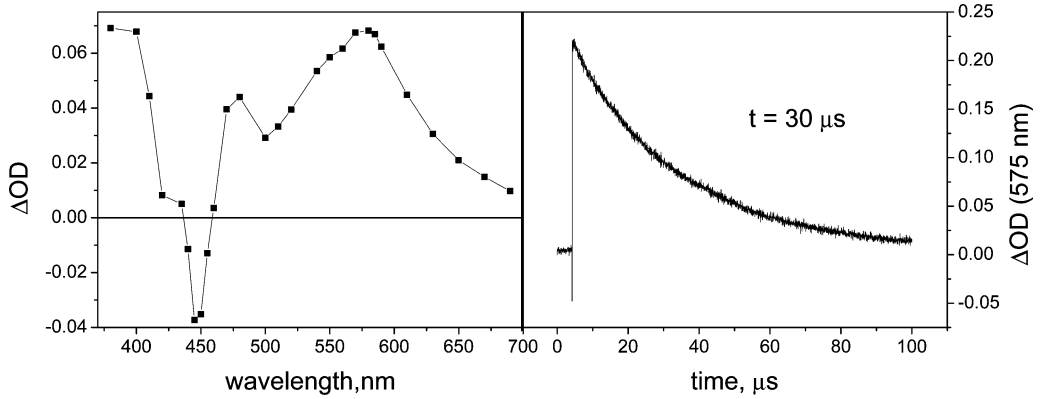

Figure 9. Laser flash photolysis of the Zn−tatpp complex in CH_3CN. Transient spectrum recorded at 50 ns delay (left); decay kinetics (right).

difference between the electrochemical potentials for (metal-centered) oxidation and (ligand-centered) reduction.[42] For $[(phen)_2Ru(tatpp)Ru(phen)_2]^{4+}$ (Table 1), oxidation takes place at a typical potential for ruthenium(II) polypyridine complexes, but reduction is easier by ca. 0.6 and ca. 1.0 V with respect to $[(phen)_2Ru(tpphz)Ru(phen)_2]^{4+}$ and $Ru(bpy)_3^{2+}$, respectively. Thus, the MLCT absorption of $[(phen)_2Ru(tatpp)Ru(phen)_2]^{4+}$ is expected to be strongly red-shifted with respect to these model compounds, with an estimated[42] λ_{max} of ca. 700 nm. In fact, however, the main

(42) Juris, A.; Balzani, V.; Barigelletti, S.; Campagna, S.; Belser, P.; von Zelewski, A. *Coord. Chem. Rev.* **1988**, *84*, 85−277.

MLCT absorption of $[(phen)_2Ru(tatpp)Ru(phen)_2]^{4+}$ is at ca. 450 nm, i.e., practically at the same energy as that found for $[(phen)_2Ru(tpphz)Ru(phen)_2]^{4+}$ and $Ru(bpy)_3^{2+}$.

The answer to this apparent discrepancy lies in the complex electronic structure of the systems. In previous work on analogous tpphz complexes, the involvement of multiple metal-to-bridge CT states was inferred from inspection of the molecular orbitals (extended Huckel) of the tpphz ligand.[17] Similar conclusions were recently reached for tatpp complexes on the basis of molecular orbitals (PM3) on the tatpp ligand.[20] The molecular orbitals of the Ru(II) binuclear complex, obtained in this work with DFT calculations (Figure 1), illustrate the point very clearly. The lowest MLCT state involves transfer of one electron from ruthenium-localized occupied orbitals to the LUMO, i.e., to a tatpp orbital predominantly localized on the central ladder-type portion, with little electron density on the bpy-like terminal fragments. This implies a small oscillator strength for the lowest MLCT transition. At higher energy, the next pair of MLCT states involves transfer of one electron to orbitals predominantly localized on the bpy-like terminal fragments of tatpp. The corresponding MLCT transitions are thus expected to have high oscillator strength. These arguments make the interpretation of the absorption spectra straightforward. The intense absorption at ca. 450 nm arises from MLCT transitions involving high-energy tatpp-centered orbitals (possibly superimposed to MLCT transitions involving the outer phenanthroline ligands). The lowest singlet MLCT state, on the other hand, does not show up in the spectrum,[43] behaving essentially as a nonspectroscopic state.

Similar arguments can be made and similar conclusions can be reached for the Os(II) complex. The only differences are the following, as usual: (i) the red shift of all the MLCT bands, caused by the easier oxidation of the metal; (ii) the appearance of additional MLCT transitions of singlet−triplet character in the low-energy region of the spectrum, caused by the higher spin−orbit coupling of the metal.

The molecular orbitals obtained from DFT calculations are also helpful in the interpretation of the electrochemical processes of the binuclear tatpp complexes (Table 1). The two-electron oxidation process (+1.32 V in the Ru(II) tatpp species and +0.85 V for the Os(II) compound) obviously involves the pair of degenerate metal-centered HOMO orbitals. All the cathodic processes have been assigned as tatpp-centered reductions.[29] The first one-electron reduction (−0.26 and −0.07 V for the Ru and Os compounds, respectively) is easily attributed to population of the low-energy LUMO orbital. The second one-electron process (−0.75 and −0.24 V for the Ru and Os compounds, respectively) can be assigned as a second reduction at the LUMO, the cathodic shift being caused by electron repulsion within this delocalized orbital.[44] The next two-electron reduction process (−1.31 V for the Ru species and − 1.27 V for the Os species) very likely involves the quasi-degenerate bpy-like LUMO+1 and LUMO+2 orbitals. Further two-electron processes[29] occurring at more negative potentials (not shown in Table 1) probably correspond to reduction of the outer phenanthroline ligands.

Photophysical Behavior. The lack of emission from the binuclear tatpp complexes is not surprising. As a matter of fact, the analogous tpphz systems were already poor emitters, due to the low energy of their MLCT states.[20,21] The further decrease in MLCT energy experienced by the tatpp complexes (as indicated by the electrochemical data) makes emission from these species very unlikely. The results from time-resolved spectroscopy experiments can be used to define the pathways of efficient radiationless decay in these systems.

$[(phen)_2Ru(tatpp)Ru(phen)_2]^{4+}$. The $[(phen)_2Ru(tatpp)Ru(phen)_2]^{4+}$ complex is characterized (Figures 3 and 4) by very fast formation of a transient with $\lambda_{max} = 580$ nm, followed by a slower decay. The formation and the decay of this transient exhibit opposite solvent dependencies, being respectively faster and slower in CH_2Cl_2 (Figure 4) relative to CH_3CN (Figure 3). The solvent dependence of the decay kinetics is particularly striking: the transient, short-lived (few nanoseconds) in CH_3CN, has microsecond lifetime in CH_2Cl_2 (Figure 5). These results led us, in a preliminary communication about this system,[30] to assign the 580 nm transient as the lowest triplet MLCT state (indicated as a "charge-separated" state, in view of the above-mentioned LUMO localization). This assignment has to be reconsidered in the light of the new experimental results. In particular, the photophysics of the tatpp ligand (not available at the time of the preliminary communication) and the difference in behavior between the Ru(II) and Os(II) systems (vide infra) point toward a drastically different assignment.

The photophysics of the tatpp ligand (as adduct with the electronically innocent Zn ion) is straightforward. The transient observed in the laser flash photolysis (Figure 9) can be assigned with confidence to the lowest triplet state of tatpp. The long lifetime (30 μs) and the pronounced oxygen quenching are as expected for such a state. In ultrafast spectroscopy (Figure 8), the triplet state is seen to be generated by a fast (130 ps) intersystem crossing process. The important observation is that the long-lived transient obtained in the flash photolysis of tatpp (Figure 9) is identical to that observed with $[(phen)_2Ru(tatpp)Ru(phen)_2]^{4+}$ in CH_2Cl_2 (Figure 5). This result firmly establishes that the 580 nm transient observed with $[(phen)_2Ru(tatpp)Ru(phen)_2]^{4+}$ is *not* an MLCT state, but rather a tatpp LC triplet.

The occurrence of an LC triplet as the lowest excited state of the system, a rather uncommon feature in ruthenium(II) polypyridine complexes, is no doubt related to the presence of the long, fully aromatic tatpp bridge.[45] In general, increasing the length of this type of ligand is expected to

(43) A weak tail (shoulder at ca. 570 nm) is observed in the low-energy region of the spectrum. This feature is definitely too high in energy to be associated with the lowest MLCT transition (estimated λ_{max}, ca. 700 nm). Some contribution cannot be completely ruled out, however.

(44) It should be noticed that the first two tatpp-centered reductions are (i) substantially easier and (ii) less mutually spaced in the Os(II) complex than in the Ru(II) one. This is consistent with a greater extent of metal−ligand orbital mixing for the Os(II) system.

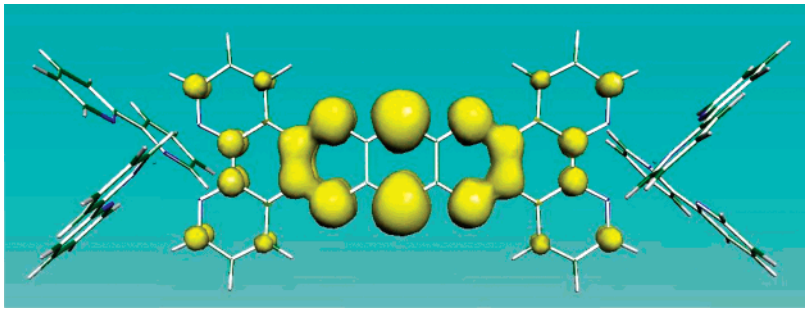

Figure 10. Spin density contour plot for the lowest triplet state of $[(bpy)_2Ru(tatpp)Ru(bpy)_2]^{4+}$.

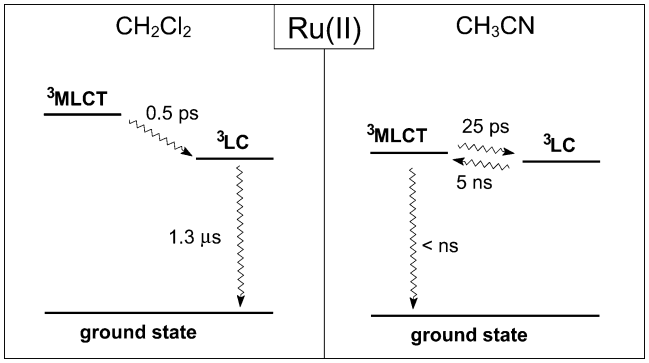

Figure 11. Qualitative energy level diagram and photochemical mechanism for $[(phen)_2Ru(tatpp)Ru(phen)_2]^{4+}$ in CH_2Cl_2 (left) and CH_3CN (right).

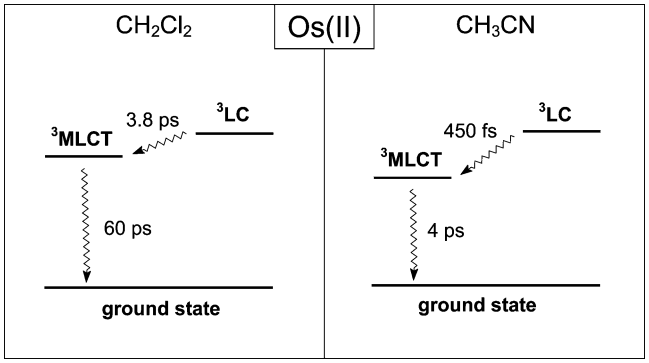

Figure 12. Qualitative energy level diagram and photochemical mechanism for $[(phen)_2Os(tatpp)Os(phen)_2]^{4+}$ in CH_2Cl_2 (left) and CH_3CN (right).

lower the energy of both MLCT and LC states, so that the prediction of the relative ordering is not obvious. As discussed above, at the singlet level the LC state is considerably higher in energy than the lowest MLCT state. The situation is evidently reversed at the triplet level, reflecting the expected larger singlet−triplet splitting of LC relative to MLCT states.

The LC nature of the lowest triplet excited state is confirmed by the DFT and TDDFT calculations. In fact, TDDFT calculations indicate that the lowest energy $S_0 \rightarrow T_1$ transition involves the HOMO-6 and LUMO orbitals,[46] which are both tatpp-localized (Figure 1). Moreover, the spin density obtained for the T_1 state by DFT calculations is largely localized on the tatpp bridging ligand (Figure 10).

Given the LC nature of the lowest excited state, an interesting question arises as to its strongly solvent-dependent decay kinetics. The interpretation is not obvious, as LC states are nonpolar and their energy is expected to be largely solvent-independent. A plausible explanation can be offered, however, if the solvent-sensitive MLCT state is considered to play a role in the deactivation of the LC state. A realistic guess at the energy situation for the two solvents used is depicted in Figure 11.

In CH_2Cl_2 the ^{3}MLCT state is sufficiently high in energy that the deactivation of the ^{3}LC state takes place independently, with an intrinsic lifetime of 1.3 μs. In CH_3CN, on the other hand, the ^{3}MLCT state is sufficiently low in energy as to be thermally accessible from the ^{3}LC state and, due to its intrinsically short lifetime (not known, but plausibly in the sub-nanosecond regime), it acts as an efficient deactivation channel. In this solvent, the lifetime of the ^{3}LC state (ca. 5 ns) is essentially determined by the rate of the activated $^3LC \rightarrow {}^3MLCT$ conversion. The formation of the ^{3}LC state from the upper MLCT and LC states of singlet multiplicity reached by light absorption is certainly a complex process. Nevertheless, it is tempting to assign the process observed in ultrafast spectroscopy to the $^3MLCT \rightarrow {}^3LC$ conversion, as the kinetics (<1 ps in CH_2Cl_2, 25 ps in CH_3CN) seems to correlate with the expected relative driving force of this step in the two solvents.

$[(phen)_2Os(tatpp)Os(phen)_2]^{4+}$. The transient behavior of $[(phen)_2Os(tatpp)Os(phen)_2]^{4+}$ (Figures 6 and 7) is qualitatively very different from that of $[(phen)_2Ru(tatpp)Ru(phen)_2]^{4+}$. It is characterized by a very fast initial *decrease* (rather than increase) in optical density in the range of 500−650 nm (Figures 6 and 7, upper left). The resulting spectrum, characterized by ground-state bleaching at 475 and 575 nm and positive absorption at 675 nm, then decays rapidly to the initial baseline (Figures 6 and 7, lower left).

Considering the substantial lowering of the MLCT states of Os(II) complexes relative to the Ru(II) analogues (the change in $E_{ox} - E_{red(1)}$ in Table 1 is almost 1 V for the tatpp systems), it is very likely that in this case the lowest excited state is, in both solvents, the ^{3}MLCT one. Thus, the transient decaying back to the baseline in the ultrafast experiments is assigned to this state. Such a situation is sketched in Figure 12. The solvent sensitivity of the decay kinetics (60 ps in CH_2Cl_2, 4 ps in CH_3CN) is consistent with the expected solvent effect on the ^{3}MLCT energy and the energy-gap law for radiationless decay. The formation of the ^{3}MLCT state from the upper MLCT and LC states of singlet multiplicity reached by light absorption is certainly, again, a complex

(45) Ligand-centered triplets have been theoretically proposed as lowest energy excited states for related Ru(II) mononuclear complexes.[27]

(46) This conclusion holds regardless of whether the TD/DFT calculation is performed at S_0 or T_1 optimized geometry.

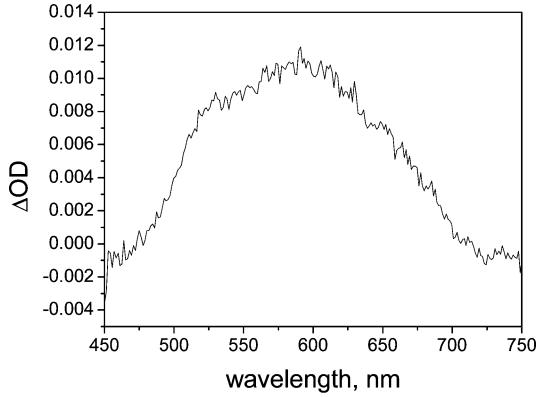

Figure 13. Difference between the spectra taken at 1.7 and 9.0 ps in Figure 7.

process. The decrease in optical density observed in the early spectral changes indicates the disappearance of a species with λ_{max} of ca. 580 nm (Figure 13).

Since this spectrum matches reasonably well that of the ^{3}LC state in the Ru(II) system and free tatpp (Figures 5 and 9), the observed process can be tentatively assigned to the ^{3}LC → ^{3}MLCT conversion (Figure 13). The kinetics (3.8 ps in CH_2Cl_2, 0.45 ps in CH_3CN) correlates well with the relative driving force of this step in the two solvents.

Conclusions

In this work, a thorough photophysical study of the Ru(II) and Os(II) homo-binuclear complexes of the tatpp bridging ligand leads to unambiguous assignments for the low-lying excited states. The comparison with previous results on analogous systems involving the shorter tpphz bridge provides a clear picture of the effects of bridge elongation on the excited-state properties of this class of ladder-type aromatic bridges.

With many bridging ligands, the photophysical behavior of binuclear Ru(II) and Os(II) complexes is qualitatively homogeneous, being dominated by low-lying MLCT states of triplet character.[6] The main differences between the Ru(II) and Os(II) systems are quantitative, particularly in the MLCT state lifetime being shorter for the Os(II) system because of lower excited-state energy (energy-gap law). In the case of polyquinoxaline bridges, this general behavior holds true for complexes of the shortest member of the series, tpphz.[20,21,24]

When the longer tatpp systems are considered, however, the behavior of the Ru(II) complex differs dramatically from that of the Os(II) one. The reason lies in the increased delocalization of the tatpp bridge relative to tpphz. This lowers in energy not only the MLCT triplet state but also (and to a greater extent) the LC triplet state, leading, in the case of Ru(II), to excited-state inversion (Figure 14). Such an inversion is not effective in the case of Os(II) because of the intrinsically lower MLCT energy. The consequence is that the nature of the lowest excited state is different for the two tatpp complexes: LC for the Ru(II) complex, MLCT

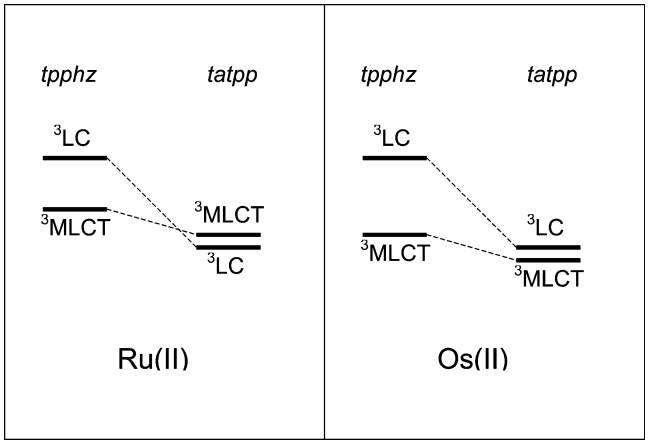

Figure 14. Qualitative representation of the effects of bridge elongation (from tpphz to tatpp) on the low-lying excited states of Ru(II) and Os(II) binuclear complexes.

for the Os(II) one. This energy situation is further fine-tuned by the solvent dependence of the MLCT energy, which causes relevant solvent effects on the photophysics of both species (Figures 11 and 12).

Ladder-type aromatic bridges are promising candidates for possible applications as molecular wires. From this viewpoint, the results of this work highlight an important feature: elongation of the bridge causes the LC triplet to substantially drop in energy and, at some point, to become the lowest excited state of the system. This is no problem for molecular electronics applications, where the molecular wire is ideally connected to electrodes. On the other hand, the presence of an LC triplet acting as an energy sink may be a major drawback from the molecular photonics viewpoint, when excited chromophores are used for electron injection into the wire.[47]

With the extended aromatic tatpp bridging ligand, complexes of Ru(II) and Os(II) have different types of lowest triplet excited state: ligand-centered in the case of Ru(II), metal-to-ligand charge transfer in the case of Os(II).

Acknowledgment. Financial support from MIUR (Projects PRIN 03 and FIRB-RBNE019H9K), the EC (Grant G5RD-CT-2002-00776, MWFM), ACS-PRF AC (F.M.M.), the Robert A. Welch Foundation (F.M.M.), and the National Science Foundation (Grant CHE-0101399 (F.M.M.)) is gratefully acknowledged. We also thank Dr. Norma de Tacconi for experimental assistance.

Supporting Information Available: Details of optimized geometries and MO energies (pdf). This material is available free of charge via the Internet at http://pubs.acs.org.

IC051062Z

(47) It should be noticed, however, that complexes of the bqpy bridge (Chart 1) were found to exhibit a relatively low degree of electron delocalization.[18] This could suggest inclusion of angularly fused rings as a possible way to avoid formation of low-energy sinks in long ladder-type bridges.